Berg Huettenmaenn Monatsh (2024) Vol. 169 (1): 31–37
https://doi.org/10.1007/s00501-023-01425-5

BHM Berg- und Hüttenmännische Monatshefte

Fatigue Behaviour of an Additively Manufactured Drive Wheel Made of Ti6AL4V

Deborah Kaschube[1,2] and Berend Bohlmann[1]

[1]Faculty of Mechanical Engineering, Kiel University of Applied Sciences, Kiel, Germany
[2]Department of Mechanical and Electrical Engineering, University of Southern Denmark, Odense, Denmark

Received November 9, 2023; accepted December 14, 2023; published online January 15, 2024

Abstract: This contribution investigates the fatigue behaviour of a newly designed drive wheel made of Ti6Al4V using cold metal fusion. In addition to its actual task, the new drive wheel also serves as a spring element to cushion force peaks caused by the application and thus protect surrounding components. The special design with integrated spokes and stop points allows for a rotation within the drive wheel of 2.9°. The entire wheel was subjected to shape, strength, weight, and function optimisation by means of topology optimisation and specially designed for additive manufacturing using cold metal fusion. Previous tests on small specimens provide the necessary material parameters to carry out a strain life fatigue strength simulation. The simulation was validated by means of component tests on the test bench and in the vehicle.

Keywords: Cold metal fusion, Low-cycle fatigue, Ramberg-Osgood law, Finite element simulation, Smith Watson Topper damage parameter

Ermüdungsverhalten eines additiv gefertigten Antriebsrads aus Ti6AL4V

Zusammenfassung: In diesem Beitrag wird das Ermüdungsverhalten eines neu konstruierten Antriebsrades aus Ti6Al4V untersucht, welches mit dem cold metal fusion Verfahren hergestellt wurde. Das neue Antriebsrad dient neben seiner eigentlichen Aufgabe auch als Federelement zur Abfederung von anwendungsbedingten Kraftspitzen und damit zum Schutz umliegender Bauteile. Das spezielle Design mit integrierten Speichen und Anschlagpunkten ermöglicht eine Drehung innerhalb des Antriebsrades von 2,9°. Das gesamte Rad wurde mittels Topologieoptimierung einer Form-, Festigkeits-, Gewichts- und Funktionsoptimierung unterzogen und speziell für die additive Fertigung im cold metal fusion Verfahren ausgelegt. Vorherige Tests an Kleinproben liefern die notwendigen Materialparameter, um eine Simulation der Betriebsfestigkeit durchzuführen. Die Simulation wurde anhand von Bauteilversuchen am Prüfstand und im Fahrzeug validiert.

Schlüsselwörter: Cold metal fusion, Low-Cycle Fatigue, Ramberg-Osgood-Gesetz, Finite-Elemente-Simulation, Smith-Watson-Topper-Schädigungsparameter

1. Introduction

Free market requirements combined with shorter product lifecycles are driving the need for more efficient product design for shape and weight. Conventional manufacturing processes such as machining or casting cannot meet the increased requirements for many functionally or shape-optimised components. As a result, new technologies are being used in product design and manufacturing. Additive manufacturing (AM) enables greater freedom to create forms, making it possible to manufacture complex parts. This is why AM is growing in importance where complex shapes are needed, particularly in aerospace [1–3], medical [2, 4], and automotive [5] industries.

Due to the complex shape of the parts and the contamination of the waste with e.g. cutting fluid, up to 95% of the raw material might end up as non-recyclable waste [6] in certain cases. In addition, the commodity prices for metals have risen sharply in the wake of the pandemic in 2020 to 2022 [7]. For this reason, weight optimisation and, above all, near-netshape production of the components are becoming increasingly important. Additive manufacturing offers excellent opportunities here.

In this particular case, however, optimising the function of the component was much more important than reducing the mass. As part of the research project "FATiG—Form-optimierte Additive Fertigung von Titanbauteilen unter

D. Kaschube (✉)
Faculty of Mechanical Engineering,
Kiel University of Applied Sciences,
24149 Kiel, Germany
deborah.kaschube@fh-kiel.de

Betrachtung der Gesamtlebensdauer", additive manufacturing was used to completely rethink a component of a 45 km/h (max. speed) electric scooter that had previously been manufactured conventionally. The conventionally milled aluminium drive wheel is one of the main components of the drive unit. With the previous conventional component, overloads occurred due to force peaks which resulted in the failure of surrounding components. The complete change of the drive wheel and the integration of the function as a spring element leads to a significant improvement. In order to ensure the long-term safe operation of the new component, fatigue tests are carried out on small scale samples to obtain material parameters. These are used to predict the fatigue life of the component in a finite element simulation. The simulation is validated by means of fatigue tests of the drive wheel. It is shown that the fatigue life prediction by means of a damage parameter curve and cyclic stress-strain curve is applicable and that a simulation predicts the fatigue life sufficiently accurately without further experiments on the component.

2. Materials

The cold metal fusion (CMF) printing process is a powder-based process. Here, titanium powder is coated with a very thin layer of a binder. This modified powder is gradually applied to the print bed in layers. After a layer has been applied, a low-energy laser is used to melt the polymer coating of the titanium powder particles at specific locations in order to bond the powder particles together at these locations (see Fig. 1). In this way, the so-called green part is formed layer by layer. This is then removed from the powder bed, and loosely adhering powder is carefully removed. The remaining powder of the print bed can be reused due to the low temperature of the laser. After depowdering, the binder in the component is chemically removed and the component is then sintered in a sintering furnace. In this process, the component is slowly heated in an inert atmosphere and when the sintering temperature is reached, the titanium particles join together by diffusion processes to form a consolidated component. During this process, the component shrinks.

The printer used in this work is an EOS P110 Velocis printer. The titanium alloy Ti6Al4V grade 5 powder from Headmade Materials consisted of particle sizes of 0–25 µm.

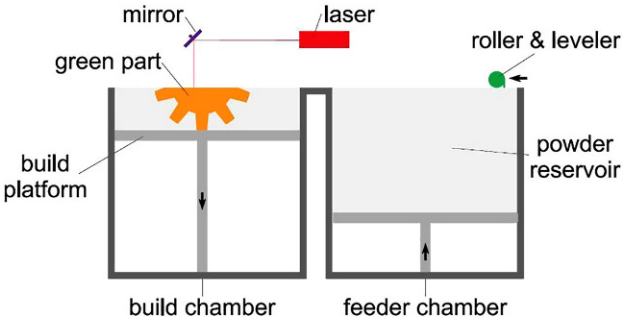

Fig. 1: Schematic of the cold metal fusion printer

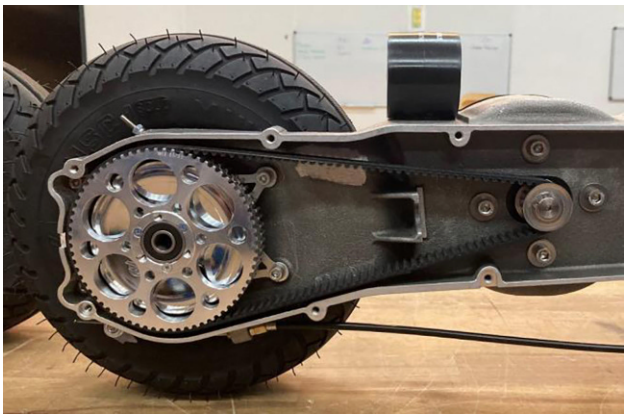

Fig. 2: Previous belt wheel mounted in the motor unit

The component optimized in this contribution is the output-side toothed belt wheel of an electric scooter with a speed of up to 45 km/h. It has a power rating of 2 KW and a rotational speed of 4000 rpm. The drum brake is mounted on it. Figure 2 shows the previous component made of aluminium installed in the motor unit. With the previous setup, material failure occurred in the past in certain driving situations, especially when driving off a curb. Even though the average curb height is only 12 cm and the drop time is low (0.156 s), this time is sufficient for the motor to reach the highest motor speed due to the loss of ground contact. During the following ground contact, the wheel is abruptly decelerated, causing surrounding components, especially the belt, to experience a high load. To absorb this peak load, the belt wheel was fundamentally redesigned and a spring effect was added. 45 spokes with a thickness of 1 mm provide rotational flexibility without losing translational stiffness. Three stiff stops, which engage at a rotation angle of 3°, ensure that the spokes are protected in extreme load cases. Figure 3 shows the new belt wheel.

The entire design was optimized in nine iteration stages with regard to additive manufacturing. The threads for mounting the drum brake are designed in a way that they only have to be recut once after sintering. The spoke thickness was limited to a minimum of 1 mm, as thinner components tend to break during depowdering. Wherever material is not required for reasons of strength or stiffness, it was consistently saved (see, for example, Fig. 3, inside of the sprocket). In this way, despite the higher density of titanium, weight reduction was also achieved in addition to the superficial optimization of function.

In addition to general static tests, the component's fatigue performance is determined by means of strain-life and damage parameter-life concepts. Therefore, experiments on small scale specimens in hourglass shape are carried out to establish the relevant material parameters of the sintered Ti6Al4V.

The hourglass specimen is designed according to ASTM E606 [8] and ISO 12106:2003 [9] and is a combination of flat and round specimen. Fully reversed (R = –1), sinusoidal strain-controlled uniaxial fatigue tests were carried out in

Fig. 3: Improved belt wheel

air on an electromagnetically excited Sincotec MAC100 resonance test bench.

The tests result in triplets, containing the strain amplitude ε_a, the resulting stress amplitude σ_a and the number of life cycles until failure N. The values of ε_a and σ_a are used for generation of the Ramberg-Osgood law according to [10] and [11]. The curve can be described by the following formula:

$$\epsilon_a = \frac{\sigma_a}{E} + \left(\frac{\sigma_a}{K'}\right)^{\frac{1}{n'}} \tag{1}$$

Where K' is the cyclic strength coefficient, n' is the cyclic strain hardening exponent and E the Young's Modulus of the material, which was determined to 109 GPa.

The tests also result in a damage parameter curve according to Smith, Watson, Topper [12].The damage parameter is described by:

$$P_{SWT} = \sqrt{(\sigma_m + \sigma_a \cdot \epsilon_a \cdot E)} \tag{2}$$

Where σ_m is the mean stress.

Different strain amplitudes ranging from 1.7–12.2 mm/m are tested. The resulting couples of P_{SWT} and life until failure N can be regressed to a straight line on a double logarithmic scale. The resulting straight line is expressed in the following format:

$$P_{SWT} = a \cdot N^{\frac{1}{b}} \tag{3}$$

Formula 2 and 3 can be combined to calculate the predicted life until failure using the stress results from the finite element simulation.

To reduce the computation time, it is sufficient to perform a linear finite element analysis. The linear values obtained can then be converted into elastic-plastic values using the Ramberg-Osgood law in combination with the Neuber hyperbola [13]. Klinger [14] showed that the approximate description by the Neuber hyperbola provides sufficiently accurate results for this material.

The finite element simulation is performed with the software ANSYS Workbench 2022 R2. In order to find out the critical point for the fatigue life, the entire drive wheel is modelled. A high-resolution mesh is required for the application of the notch concept. In this case, it consists of 6,173,067 elements with 8,946,873 nodes. The simulation of the force transmission from belt to wheel is based on

Fig. 4: Applied constraints

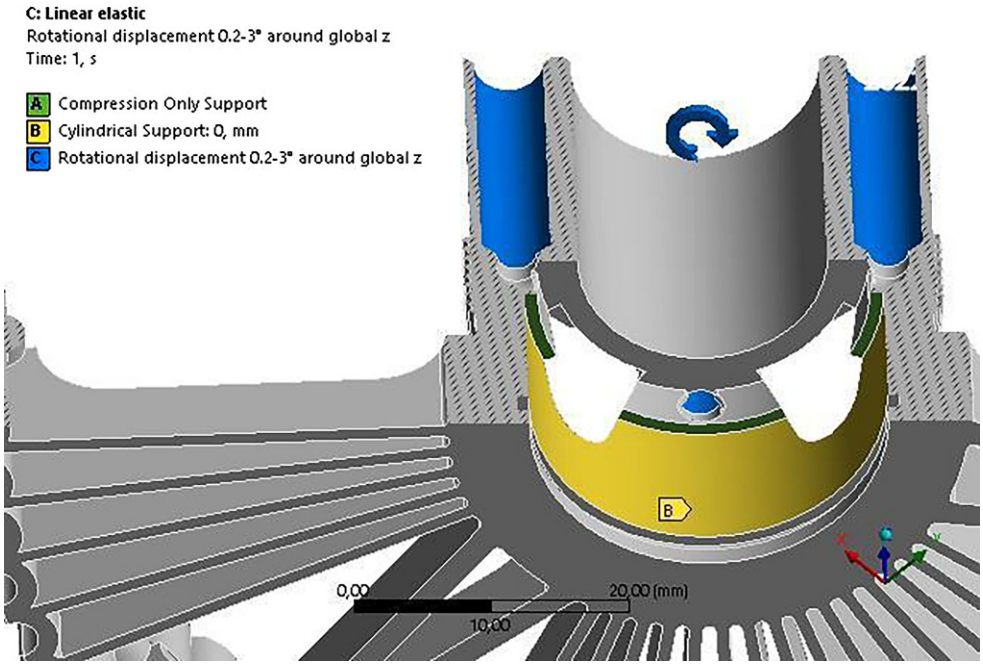

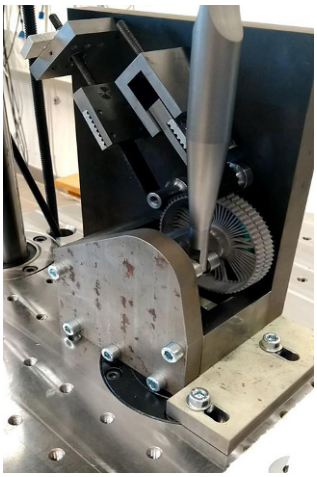

Fig. 5: Test setup

5 teeth, as in reality, due to the elongation of the belt, only few teeth carry. Figure 4 shows all applied constraints. Only a torsion angle up to 2.8° is relevant for the fatigue life consideration. The simulation increment of the rotational angle is 0.2°.

A further load case occurs when the stop buffers engage at a torsion angle greater than 2.8°. This is analysed separately as a static event, since this case does not occur in normal use.

For the components fatigue tests, wheels were printed without stop buffers. The component tests are carried out on a PowerSwingly 5Mot resonance test bench. The test setup is shown in Fig. 5. The wheel is held in place by five teeth by means of a spring assembly which tensions the belt. A torque is applied to the gear via a cam shaft. The angle is measured by means of an inductive distance sensor IF6029 by ifm. The signal from the sensor is used for angle control. The rotational angle reaches from zero to up to 4° in each load cycle. The amplitude is kept constant during the test. The force is measured with an Interface load cell 1010ACK-5 kN. The rupture of a spoke is detected acoustically and taken as the failure criterion. The acoustic signal of the spoke fracture is detected to be at about 3.3 kHz by FFT-analysis. It is recorded in order to be able to plot the exact number of load cycles up to the fracture. In this way, a pair of values consisting of angle and the number of load cycles until failure is obtained for each test.

3. Results

The results of the small-scale tests serve as a basis for the simulation. The Smith, Watson, Topper damage curve is shown in Fig. 6, the Ramberg-Osgood curve used for the extrapolation by means of Neuber hyperbola is shown in Fig. 7. The values of both curves can be taken from Table 1. For further reference of the small scale test results, see [16].

The results of the simulation show that the wheel experiences the greatest stresses at the inner positions of the spokes. As the simulation is linear, this applies for all the rotation angles. Figure 8 shows in detail the highest equivalent stress when the wheel is rotated by 2.8°. The values of the equivalent stress at a rotation angle of 0.2–2.8° are shown in Table 2 together with the elastic-plastic stress and strain values determined from this by means of the Ramberg-Osgood curve and the Neuber hyperbola. This table also shows the values for P_{SWT} and N_f calculated by means of formulae (2) and (3).

A broken spoke was the cause of the failure in all the wheels tested, see Fig. 9. The number of load cycles until failure is shown for the tested angles in Fig. 10. This figure also compares the results from the tests with those from the simulation.

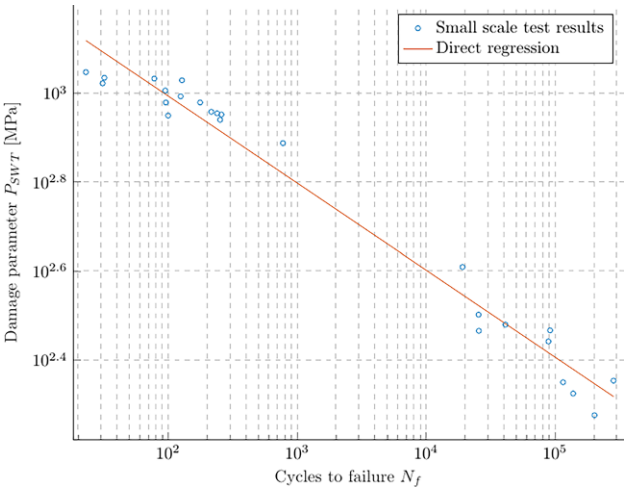

Fig. 6: Experimental data and fitted P_{SWT} curve using linear regression method suggested by Wächter [15]

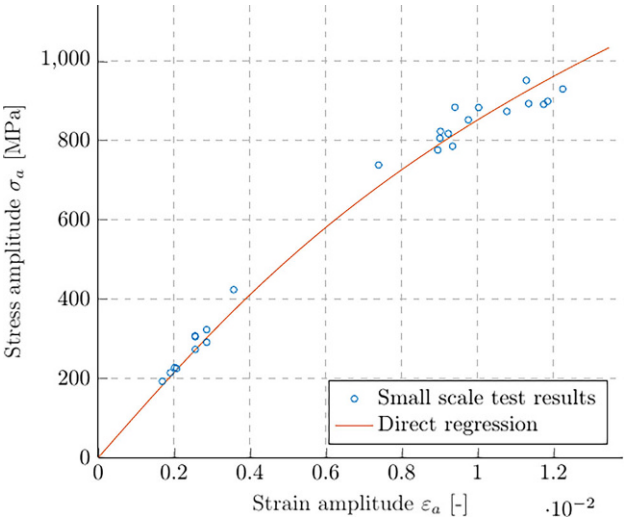

Fig. 7: Experimental data and fitted Ramberg-Osgood curve using linear regression method suggested by Lee [10]

TABLE 1
Damage parameter curve and Ramberg-Osgood curve parameters

$E\left[\frac{N}{mm^2}\right]$	$a\left[\frac{N}{mm^2}\right]$	b [–]	$K'\left[\frac{N}{mm^2}\right]$	n' [–]
109,000	2423.8	–5.1103	6201	0.3241

TABLE 2
Simulation results and calculated values for P_{SWT} and N_f

Angle [°]	$\sigma_{el_{max}}$ [MPa]	σ_{max} [MPa]	ε_a [10^{-3}]	P_{SWT} [MPa]	N_f
0.2	51.12	51.10	0.235	36.14	2,156,789,655
0.4	102.30	102.13	0.469	72.29	62,419,857
0.6	153.56	152.96	0.705	108.42	7,865,339
0.8	204.95	203.52	0.942	144.54	1,810,007
1	258.57	255.68	1.189	182.06	556,463
1.2	313.34	308.21	1.443	220.19	210,584
1.4	369.28	360.95	1.704	258.89	92,055
1.6	426.55	413.89	1.972	298.24	44,672
1.8	485.16	466.87	2.248	338.20	23,494
2	545.18	519.82	2.532	378.79	13,164
2.2	606.68	572.67	2.826	420.03	7763
2.4	669.78	625.40	3.131	461.98	4773
2.6	734.42	677.86	3.446	504.58	3041
2.8	800.61	729.98	3.772	547.83	1998

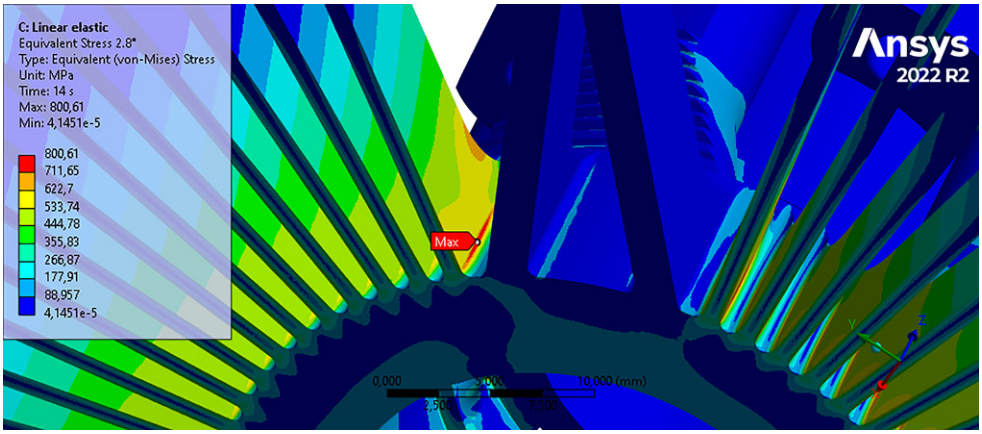

Fig. 8: Equivalent stress at a rotation angle of 2.8°

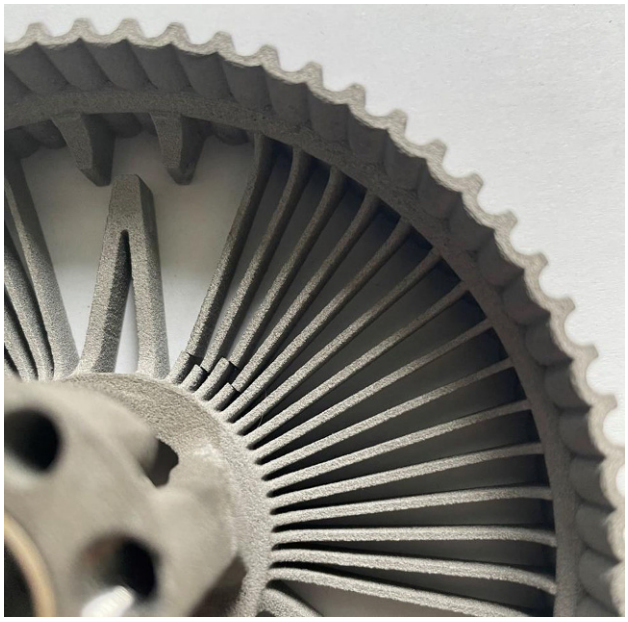

Fig. 9: Location of fracture exemplarily shown at one of the tested wheels

4. Discussion

The crack location at the lower end of a spoke determined in the simulation occurs in the same way in the test. Figure 10 shows in the simulation the expected linear course of the fatigue life over the angle on a double-logarithmic scale. The four evaluated tests also indicate a slightly upward parallel shifted straight line. However, this still needs to be confirmed by tests at smaller angles. Overall, failure occurs later in the test than predicted by the simulation, e.g. the simulations provide conservative results. However, this large silent safety is not desirable. A possible cause is currently under investigation. After conducting the tests, it was found that the spokes were under compressive stress (see Fig. 9, shear of the broken ends relative to each other).

This might result from the cooling behaviour of the selected component. Due to the different thicknesses, the wheels do not equally cool down but faster in thin areas, i.e. the spokes. During the subsequent cooling of the sprocket, this could result in exerting pressure on the spokes and thus secondary stresses in the spokes. The compressive stress would improve the fatigue performance because it

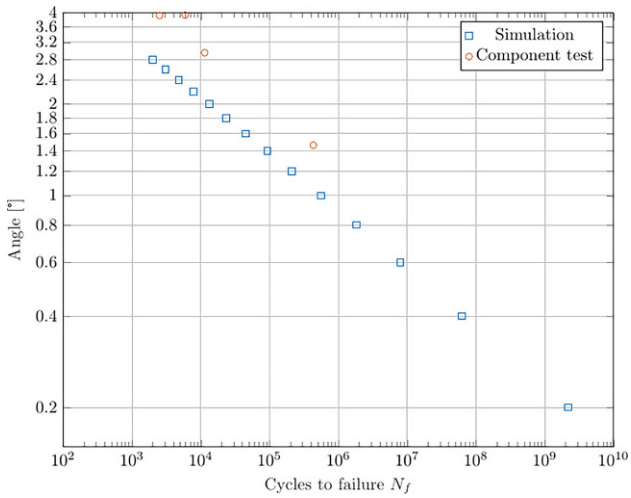

Fig. 10: Life until failure plotted over the angle of rotation-simulation and component test results

remarkably reduces the primary tensile stresses. In order to support the hypothesis, simulations of the cooling behaviour and measurements on untested components are currently being carried out. In this specific case, the residual stresses are "good", but in other geometries they might have negative impact.

5. Conclusion

The following conclusions and future tasks result from the work presented here:

- The spokes of the investigated component were probably under compressive residual stress due to the manufacturing process. The degree to which this is responsible for the improved performance in the tests still needs to be investigated.
- The component was tested under laboratory conditions at constant amplitude loading. The component was additionally installed in a complete exhibition drive unit and here also subjected to a constant amplitude load. Here, too, it was found to have an extended fatigue life compared with the simulation.
- The component is currently being tested in a pre-series vehicle under real conditions. The results are still pending, but will provide important insights into the behaviour under real alternating load conditions.

In summary, the notch concept performs sufficiently for the prediction of the fatigue performance of CMF manufactured components. It is likely, that more attention should be paid to different rapid resp. slow cooling down of the different thickness areas of the component in order to avoid residual stresses.

Funding. This work was supported by the European Regional Development Fund (ERDF), the Federal Republic of Germany, and the state of Schleswig-Holstein.

Funding. Open Access funding enabled and organized by Projekt DEAL.

Conflict of interest. D. Kaschube and B. Bohlmann declare that they have no affiliation with or involvement in any organization or entity with any financial or non-financial interest in the subject matter or materials discussed in this manuscript.

References

1. Lasagni, F., Vilanova, J., Periñán, A., Zorrilla, A., Tudela, S., Gómez-Molinero, V.: Getting confidence for flying additive manufactured hardware. Prog Addit Manuf **1**(3–4), 129–139 (2016). https://doi.org/10.1007/s40964-016-0014-7
2. Grund, M.: *Implementierung von schichtadditiven Fertigungsverfahren: Mit Fallbeispielen aus der Luftfahrtindustrie und Medizintechnik* (Light Engineering für die Praxis). Berlin: Springer Vieweg (2015). http://search.ebscohost.com/login.aspx?direct=true&scope=site&db=nlebk&AN=1079704, Accessed Online
3. Airbus. "Large-scale 3D printing goes to space on Airbus' Eurostar Neo satellites." https:// www.airbus.com/en/newsroom/stories/2021-02-large-scale-3d-printing-goes-to-space-on-airbus-eurostar-neo-satellites (accessed Apr. 26, 2022).
4. I. Buj-Corral, A. Tejo-Otero, and F. Fenollosa-Artés, "Development of AM Technologies for Metals in the Sector of Medical Implants," *Metals*, vol. 10, no. 5, p. 686, 2020, https://doi.org/10.3390/met10050686.
5. Wörner, S., Jung, U., Friederich, H., Beier, H.T., Vormwald, M.: Rapid Prototyping im Maschinen- und Automobilbau – Ermüdungseigenschaften additiv gefertigter Bauteile. In: (ed.) *Additive Fertigung von Bauteilen und Strukturen*, H. A. Richard, B. Schramm, and T. Zipsner, pp. 1–20. (2017)
6. Denkena, B., Dittrich, M.-A., Jacob, S.: Energy Efficiency in Machining of Aircraft Components. Procedia Cirp **48**, 479–482 (2016). https://doi.org/10.1016/j.procir.2016.03.155
7. International Monetary Fund, M. Stuermer, and N. Valckx. "Four Factors Behind the Metals Price Rally." https://www.imf.org/en/Blogs/Articles/2021/06/08/four-factors-behind-the-metals-price-rally (accessed Aug. 30, 2023).
8. *Test Method for Strain-Controlled Fatigue Testing*, E08 Committee, West Conshohocken, PA, 2020.
9. *ISO 12106:2003—Metallic materials—Fatigue testing—Axial-strain-controlled method: Metallic materials—Fatigue testing—Axial-strain-controlled method*, 12106, ISO—International Organization for Standardization, Geneva, 2003.
10. Lee, Y.-L.: Fatigue Testing and Analysis. Elsevier (2005)
11. Ramberg, W., Osgood, W.R.: "Description of stress-strain curves by three parameters: Technical Note. No, vol. 902. National Advisory Committee for Aeronautics, Wshington (1943)
12. Smith, R.N., Watson, P., Topper, T.H.: A stress-strain parameter for the fatigue of metals. J. Mater. , (1970)
13. Neuber, H.: no. 7. "Über die Berücksichtigung der Spannungskonzentration bei Festigkeitsberechnungen," Kontruktion im Maschinen-, Apparate- und Gerätebau, vol. 20., pp. 245–251 (1968)
14. Klinger, M.: Non-linear finite element analysis to estimate the fatigue strength of a belt pulley. Master Thesis Kiel Univ. Appl. Sci. (2022)
15. Wächter, M.: "Zur Ermittlung von zyklischen Werkstoffkennwerten und Schädigungsparameterwöhlerlinien," Fakultät für Mathematik/Informatik und Maschinenbau. Technische Universität, Clausthal, Clausthal (2016)

16. Kaschube, D., Pawlowitz, T., Solterbeck, C. H., Schloesser, J., Malekan, M., & Bohlmann, B. (2023). Fatigue behavior of Ti-6Al-4 V alloy manufactured by cold metal fusion. Fatigue & Fracture of Engineering Materials & Structures.